iScience

CellPress
OPEN ACCESS

Article

# Moderate Changes in $CO_2$ Modulate the Firing of Neurons in the VTA and Substantia Nigra

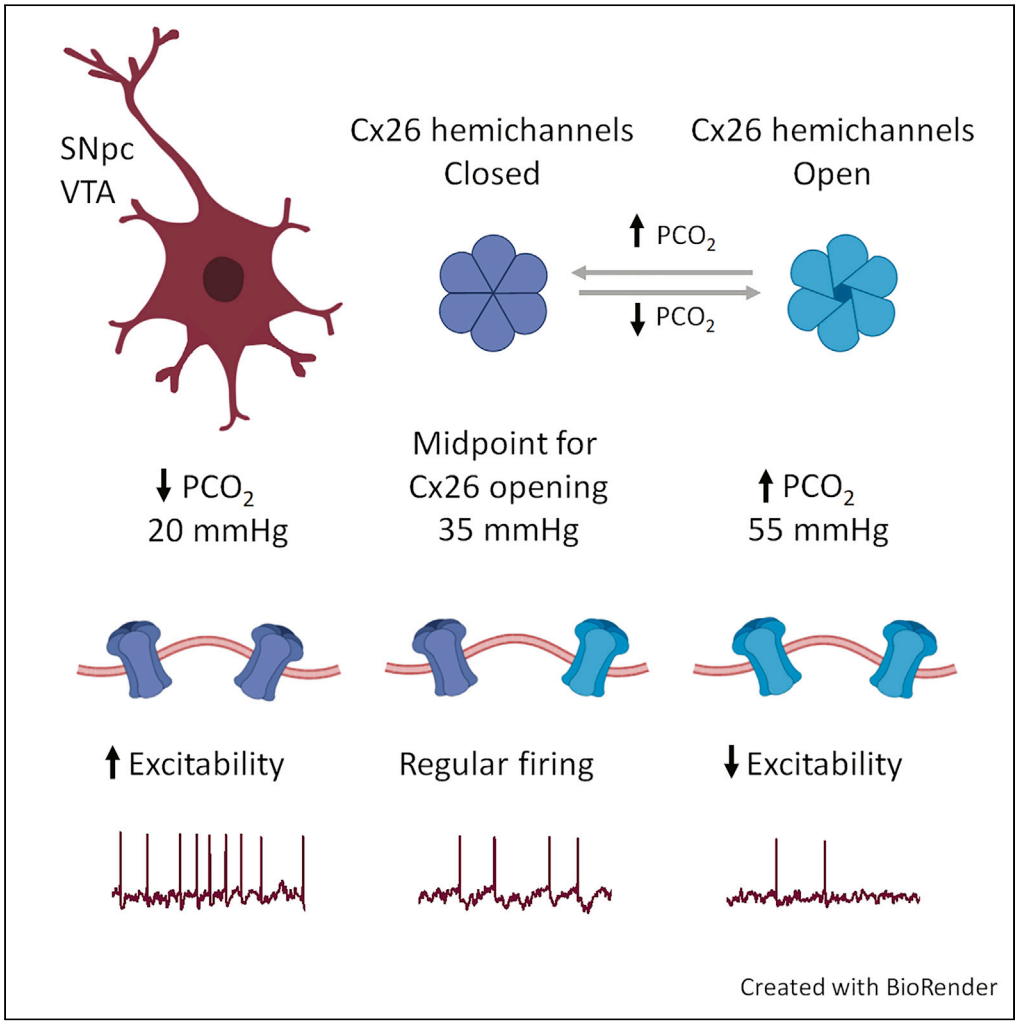


Emily Hill,
Nicholas Dale,
Mark J. Wall

e.hill.2@warwick.ac.uk (E.H.)
mark.wall@warwick.ac.uk
(M.J.W.)

## HIGHLIGHTS

The substantia nigra (SN) and VTA are key to movement and goal-directed behavior

Activity in specific SN and VTA neurons is modulated by physiological changes in $CO_2$

The neuronal $CO_2$ sensitivity results from connexin 26 (Cx26) hemichannel expression

Minute-to-minute changes in $CO_2$ could modify motor activity and reward behavior

Hill et al., iScience *23*, 101343
July 24, 2020 
https://doi.org/10.1016/j.isci.2020.101343

iScience

CellPress
OPEN ACCESS

Article

# Moderate Changes in $CO_2$ Modulate the Firing of Neurons in the VTA and Substantia Nigra

Emily Hill,[1,2,*] Nicholas Dale,[1] and Mark J. Wall[1,*]

## SUMMARY

**The substantia nigra (SN) and ventral tegmental area (VTA) are vital for the control of movement, goal-directed behavior, and encoding reward. Here we show that the firing of specific neuronal subtypes in these nuclei can be modulated by physiological changes in the partial pressure of carbon dioxide ($PCO_2$). The resting conductance of substantia nigra dopaminergic neurons in young animals (postnatal days 7–10) and GABAergic neurons in the VTA is modulated by changes in the level of $CO_2$. We provide several lines of evidence that this $CO_2$-sensitive conductance results from connexin 26 (Cx26) hemichannel expression. Since the levels of $PCO_2$ in the blood will vary depending on physiological activity and pathology, this suggests that changes in $PCO_2$ could potentially modulate motor activity, reward behavior, and wakefulness.**

## INTRODUCTION

Carbon dioxide ($CO_2$) is a waste product of cellular metabolism with its concentration in blood a major regulator of breathing. In humans, $PCO_2$ in blood is normally ~40 mm Hg but can be increased in conditions such as chronic obstructive pulmonary disease (COPD) and sleep apnea and can be decreased by hyperventilation and prolonged physical exertion. According to traditional consensus, $CO_2$ is detected via the consequent change in pH, and pH is a sufficient stimulus for all adaptive changes in breathing in response to hypercapnia (Loeschcke, 1982). pH-sensitive ion channels and receptors have been proposed to play a role in respiratory chemosensing in both the periphery (carotid body) and centrally in the medullary chemosensory areas such as the retrotrapezoid nucleus and the medullary raphe (Trapp et al., 2008; Kumar et al., 2015; Wang et al., 2013; Hosford et al., 2018). pH sensing via ventral medullary glial cells may also contribute to the $CO_2$-dependent regulation of breathing (Gourine et al., 2010; Turovsky et al., 2016). However, there is considerable evidence that $CO_2$ can have additional independent effects from pH on central respiratory chemosensors (Eldridge et al., 1985; Shams, 1985). $CO_2$ directly binds to connexin 26 (Cx26) via a structural motif, which results in carbamylation of Lys125, thus increasing hemichannel opening probability (Huckstepp et al., 2010a; Meigh et al., 2013). The midpoint for the binding is ~40 mm Hg, which, as indicated above, is the resting level in human blood, and thus small changes in $PCO_2$ will shift the open probability of Cx26 hemichannels. Pharmacological evidence suggests that Cx26 contributes to the $CO_2$-dependent regulation of breathing (Gourine et al., 2005; Huckstepp et al., 2010b; Wenker et al., 2012), and this has recently gained support from genetic evidence that links binding of $CO_2$ to Cx26 to the adaptive change in breathing (van de Wiel et al., 2020).

Coupling between dopaminergic neurons (DNs) in the substantia nigra (SN) was first described by Grace and Bunney (1983) who showed that the injection of lucifer yellow dye into single cells could result in the filling of neighboring "coupled" cells, with the dye transferring through gap junctions. They confirmed this using electrophysiology. Vandecasteele (2005) validated that pairs of DNs in the SNpc are coupled by functional gap junctions and later went on to describe the connexin expression profile of SN DNs (Vandecasteele et al., 2006). They reported that, in young rodents (postnatal day 7–10), these neurons express mRNA for Cx26 and Cx30, which are sensitive to $CO_2$, but by P17–21 they only express mRNA for $CO_2$-insensitive connexins (Vandecasteele et al., 2006). This observation led us to investigate whether the DNs in the SN of young rodents (P7–10) express $CO_2$-sensitive hemichannels and thus have a $CO_2$ phenotype. We subsequently discovered an additional population of neurons, GABAergic, in the ventral tegmental area (VTA), which also appear to express Cx26 hemichannels and are sensitive to $CO_2$. Unlike the SN DNs, these neurons appear to retain their sensitivity to $CO_2$ throughout development. Our findings reveal an unexpected role for $CO_2$ in regulating the activity of these key brain regions and demonstrate a mechanism by which autonomic state could alter complex movement-related and goal-directed behaviors. This would also be the first documentation of connexin 26 hemichannel expression in neurons.

[1]School of Life Sciences, University of Warwick, Gibbet Hill, Coventry CV4 7AL, UK

[2]Lead Contact

*Correspondence: e.hill.2@warwick.ac.uk (E.H.), mark.wall@warwick.ac.uk (M.J.W.)

https://doi.org/10.1016/j.isci.2020.101343

## RESULTS

To investigate whether dopaminergic neurons (DNs) in the SN from P7–10 mice are sensitive to levels of carbon dioxide ($CO_2$), as predicted from their connexin mRNA profile (Vandecasteele et al., 2006), we made whole-cell patch clamp recordings from DNs in acutely isolated slices. Putative DNs in the SN were identified by their electrophysiological profile. DNs were identified primarily by their position in the slice and characteristic current-voltage relationship; most displayed a large sag in response to hyperpolarizing current steps (characteristic of Ih), rebound and tonic firing at rest, and a hyperpolarizing response to dopamine application (Grace and Onn, 1989; Neuhoff et al., 2002). A subset of recorded neurons were confirmed as dopaminergic when positive for the dopamine marker tyrosine hydroxylase using immunohistochemistry (Grace and Onn, 1989; Figure 1A). In order to test whether the DNs were sensitive to $CO_2$, following their identification with standard step current injections and in some neurons also the injection of naturalistic current (to measure firing rates), the level of $CO_2$ (35 mm Hg, basal level) was increased to 55 mm Hg under isohydric conditions (compensatory changes in bicarbonate concentration to maintain constant extracellular pH during the $CO_2$ stimulus, see Methods). This increase in $PCO_2$ from 35 to 55 mm Hg (hypercapnia) produced a time-dependent reduction in the tonic firing rate and a reduction in the voltage change in response to hyperpolarizing current steps (Figures 1B and 1C). Both of these effects are characteristic of an increase in resting conductance. At steady state, the response to the hyperpolarizing current steps had fallen to 70 $\pm$ 9.6% of control ($p = 0.0015$, Figures 1B and 1C), the input resistance had fallen from 380 $\pm$ 28.15 to 217 $\pm$ 27.9 MΩ ($p = 0.0027$, $n = 10$), and the tonic firing was abolished. For a subset of recordings, we tested whether it was possible to get recovery when $PCO_2$ was returned from 55 to 35 mm Hg; this was not quantified, but an example showing partial recovery of firing rate and input resistance is illustrated in Figure 1D.

These observations were not an artifact of the dialysis of the cell following whole-cell breakthrough as the cells were first allowed time to equilibrate, then standard and naturalistic currents were injected to form IV curves and to measure firing rates. In a subset of neurons, pharmacological agents such as dopamine were applied to identify the cells (~30 min to apply and wash) prior to the alteration of $CO_2$ and similar effects of changing the $CO_2$ were observed. For initial controls, the experiment was first repeated without changing the $PCO_2$ (although the solutions were still exchanged to eliminate any artifacts due to the mechanical process of solution change), and under these conditions, the resting conductance and firing rate of the neurons did not significantly change over the time course of the experiment (Figure S1). Second, the experiment was repeated with hippocampal CA1 pyramidal neurons and there was no significant change in the electrophysiological properties of these neurons with hypercapnia (voltage response was 100.3 $\pm$ 1.64% of control, $p = 0.68$, Figure S2, $n = 6$).

### Evidence That the Effects of $PCO_2$ on Cell Conductance Are due to Cx26 Hemichannel Expression

We then took a number of approaches to investigate whether the SN DN $CO_2$ sensitivity is the result of Cx26 hemichannel expression. First, as DNs in the SN of older mice (P17–21) do not express mRNA for $CO_2$-sensitive connexins (Vandecasteele et al., 2006), they should therefore be insensitive to $CO_2$ if it is connexin hemichannel dependent. Whole-cell recordings from DN in SN from P17–21 mice showed the expected changes in electrophysiological properties that have been reported (Dufour et al., 2014) to occur during postnatal development (Figure S3) but showed no significant response to increased $PCO_2$ (voltage response was 101 $\pm$ 0.9% of control, $p = 0.33$, $n = 4$, Figures 1E and 1F). Second, the effects of increasing $PCO_2$ could be blocked by the hemichannel inhibitor carbenoxolone (Meigh et al., 2013) in P7–10 slices (100 μM Figures 1G–1I, $n = 6$). Carbenoxolone incubation did alter the electrophysiological properties of neurons (as previously reported in Tovar et al., 2009), but these changes would be expected to enhance the effects of hemi-channel opening rather than occlude them.

The midpoint for $CO_2$-dependent opening of Cx26 hemichannels is around the basal level of $PCO_2$ used in these experiments (35–40 mm Hg, Huckstepp et al., 2010a). Thus, a reduction in $PCO_2$ should close Cx26 hemichannels leading to a decrease in resting conductance and a corresponding increase in firing rate. As predicted, in P7–10 SN DNs, decreasing $PCO_2$ from 35 to 20 mm Hg (hypocapnia) increased the voltage response to hyperpolarizing current steps (104 $\pm$ 1.2% of control, $p = 0.0078$) and increased the firing rate (184 $\pm$ 28.65% of control, $p = 0.015$, Figure 2) consistent with a decrease in conductance. These effects of reduced $CO_2$ were partially reversible (Figures 2A and 2B). Thus, small changes in $CO_2$, around normal resting levels (40 mm Hg), are sufficient to modulate SN DN excitability consistent with Cx26 hemichannel expression.

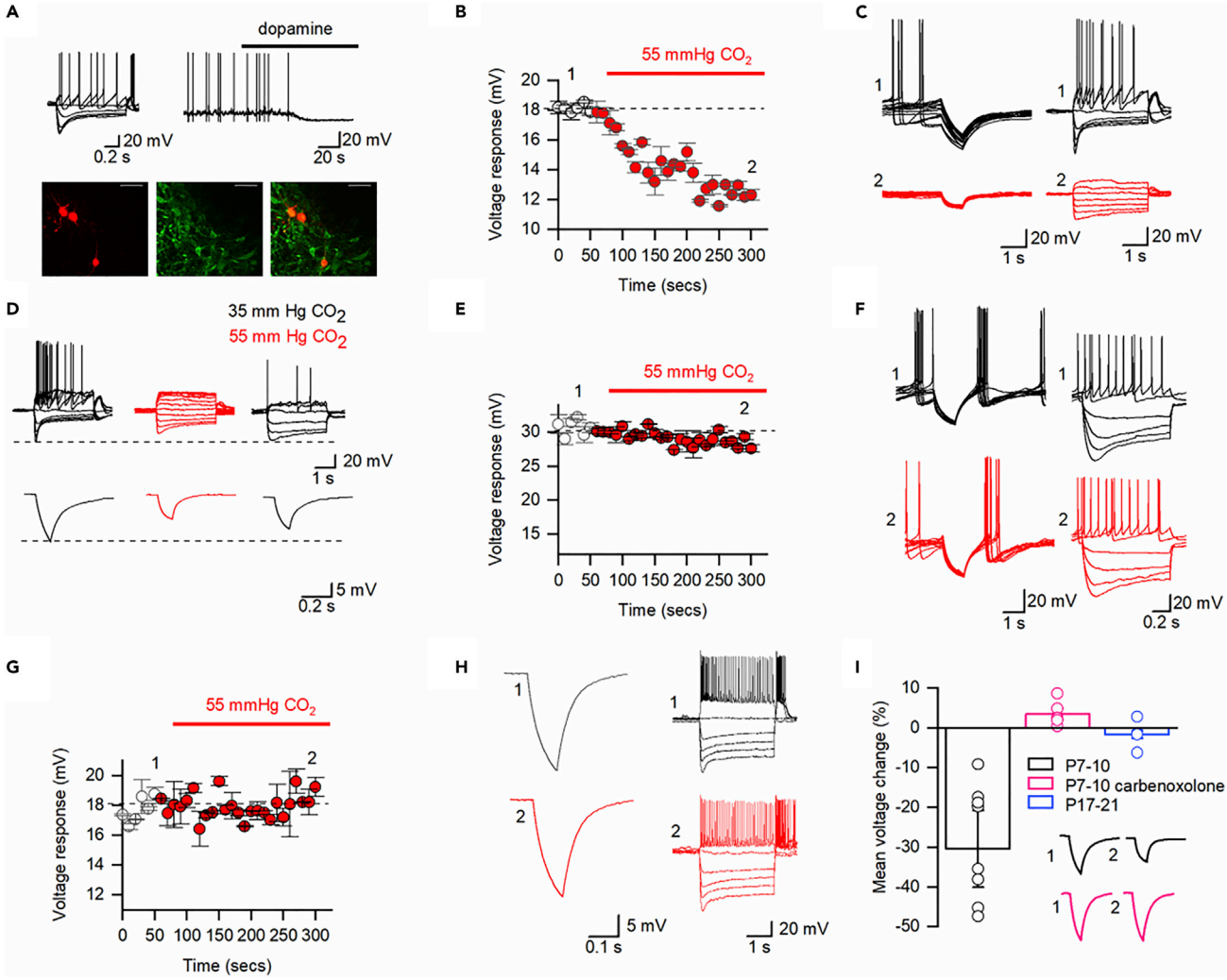


**Figure 1. $CO_2$ Sensitivity of Dopaminergic Neurons in the Substantia Nigra**

(A) Characteristic properties of SN DNs: voltage response to current injection, hyperpolarization in response to dopamine (30 μM) and recorded neurons (red) are $TH^+$ (green). Scale bar, 100 μM.

(B) Time course of changes in voltage response (P7–10, each point is a mean of six current steps, error bars are SEM) when $CO_2$ was changed from 35 to 55 mm Hg.

(C) Associated voltage traces (40 superimposed traces) and voltage responses to step currents at indicated time points from (B).

(D) Representative voltage responses (P7–10) demonstrating input resistance and firing rate changes can be partially reversed (bottom traces are an average of 25 sweeps).

(E) In P17–21 DNs there was no significant change in voltage response (each point is a mean of six current steps, error bars are SEM) when $CO_2$ was changed from 35 to 55 mm Hg.

(F) Associated voltage traces (40 superimposed traces) and voltage responses to step currents at indicated time points from (E).

(G) If slices are incubated in carbenoxolone, there is no significant change in voltage response (P7–10, each point is mean of six current steps, error bars are SEM) when $CO_2$ was changed from 35 to 55 mm Hg.

(H) Associated mean voltage traces (average of 40 sweeps) and voltage responses to step currents at indicated time points from (G).

(I) Quantification of voltage response changes (35–55 mm Hg $CO_2$). Inset, control responses and responses in carbenoxolone (1, 35 mm Hg and 2, 55 mm Hg).

## Early Postnatal Substantia Nigra Dopamine Neurons Express Connexin 26 and Dye Load with Hypercapnia

We next used a different, non-electrophysiological approach to provide further evidence that P7–10 SN DNs express $CO_2$-sensitive hemichannels. A characteristic of hemichannels is that, when they open, they allow entry of membrane-impermeant fluorescent dyes into cells. Once the hemichannels close, the dye becomes trapped inside the cells (this is termed dye loading) and can then be used as a marker for cells

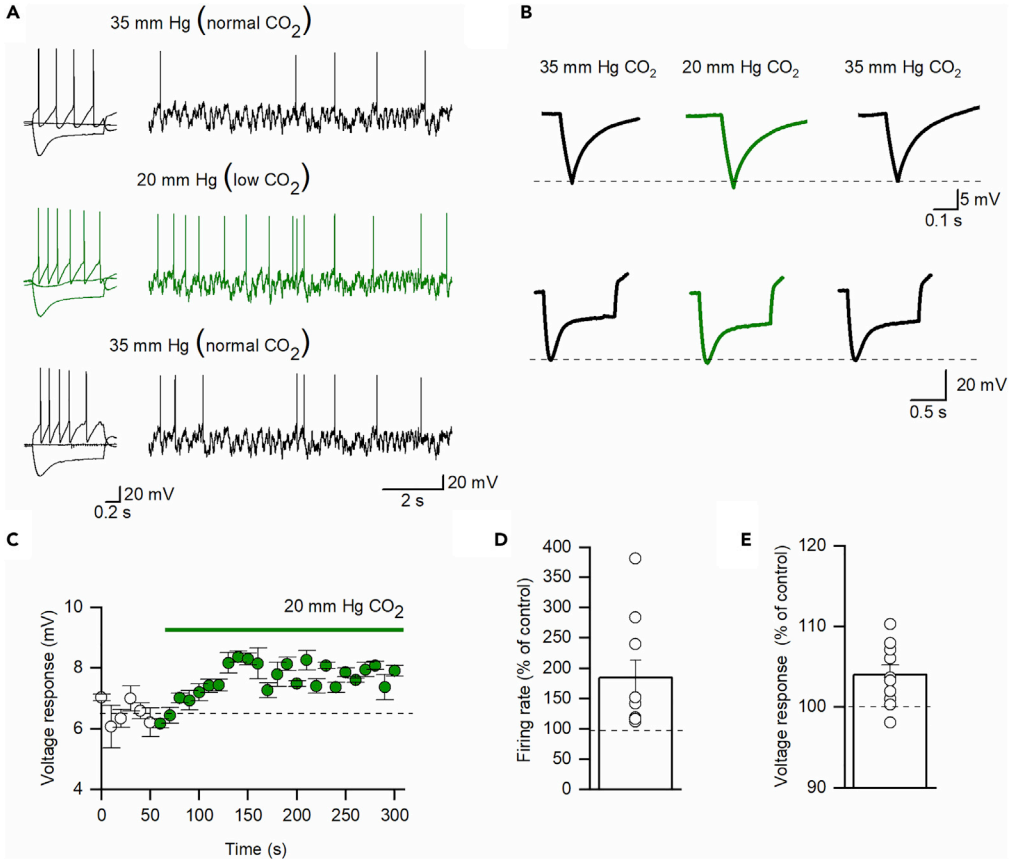


**Figure 2. P7–10 Dopaminergic Neurons in the Substantia Nigra Are Sensitive to Lowering $CO_2$**

(A) An example recording from a P7 SN dopaminergic neuron. Black traces represent recordings in 35 mm Hg (normal $CO_2$), and green traces represent recordings in 20 mm Hg (low $CO_2$). An increase in firing rate can be observed (A) from the membrane potential responses to step and fluctuating current injections (as in Badel et al., 2008; see Methods).

(B) The voltage response to a 50-pA hyperpolarizing step (top, traces are an average of 40 sweeps) and the membrane potential response to the −100-pA step injection (bottom). They show a small increase in voltage response due to increased input resistance with lowered $CO_2$. Both the left and right panels show a partial recovery of both firing rate and input resistance after washing back into 35 mm Hg $CO_2$.

(C) Time course of changes in voltage response (P7–10, each point is a mean of six current steps, error bars are SEM) when $CO_2$ was changed from 35 to 20 mm Hg.

(D) Quantification of changes to firing rate as measured by the voltage response to fluctuating current input.

(E) Quantification of the voltage response to hyperpolarizing step input. Both (D) and (E) display data normalized to the baseline values; raw data plots are available in Supplemental Information .

that express $CO_2$-sensitive hemichannels (Huckstepp et al., 2010a; Meigh et al., 2013). Grace and Bunney (1983) had previously shown that lucifer yellow can demonstrate dye coupling (into neighboring neurons from intracellular injection into a single neuron). However, Vandecasteele et al. (2006) attempted to dye load SN DNs (extracellular bath application, as described above) with lucifer yellow by opening hemichannels with low levels of $Ca^{2+}$; this was unsuccessful. We decided to use the impermeant dye carboxyfluorescein (CBF) as we could be certain that it would pass through open Cx26 hemichannels as it has been shown in previous studies (Huckstepp et al., 2010a; Meigh et al., 2013) and confirmed that neurons in the SN of P7–10 mice (Figure 3A) could be loaded with the dye following hypercapnia. No dye loading occurred if the $PCO_2$ was not increased. Dye loading did not occur in the SN of older mice (P17–21) or in CA1 hippocampal pyramidal cells (Figure S2). To further confirm that early postnatal SN DNs express connexin 26, we used a highly specific monoclonal antibody to Cx26 (Sun et al., 2009, Huckstepp et al., 2010a, 2010b). In slices from P7–10 mice, Cx26 expression was present in tyrosine hydroxylase-positive ($TH^+$) neurons in the SN (Figure 3B). However, in older mice (P17–21), Cx26 appeared not to be expressed in $TH^+$ neurons (Figure 3C). Cx26 was still expressed in the leptomeninges of corresponding sections P17–21 providing a

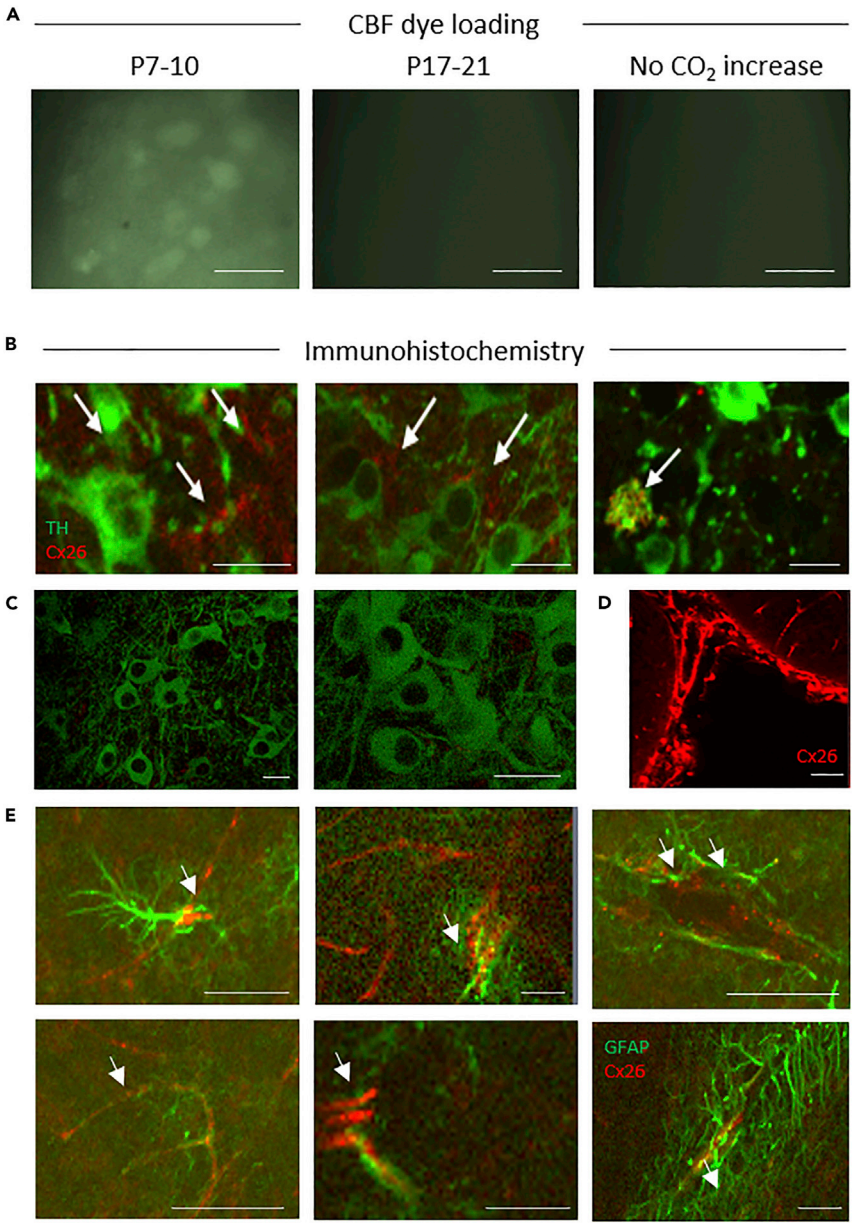


**Figure 3. Dye Loading and Cx26 Expression in Substantia Nigra**

(A) Carboxyfluorescein (CBF) dye loading following hypercapnia in P7–10 slices (cell bodies are clearly labeled). No dye loading occurred if $CO_2$ was not changed or in P17–21 slices; scale bar, 50 μM.

(B) Immunofluorescent staining of P7–10 SN for Cx26 (red, arrows) in $TH^+$ neurons (green).

(C) No co-localization of Cx26 (red) in $TH^+$ neurons (green) in the SN at P17–21; scale bars, 30 μM. Staining was deemed successful due to the positive leptomeninges staining from corresponding sections of the same brain.

(D) Scale bar, 50 μM. (E) Cx26 (red, arrows) co-localized with GFAP (green, glial cell marker) in P17–21 SN; scale bar, 50 μM.

positive control for the labeling protocol (Figure 3D). At P17–21, Cx26 sensitivity appeared to shift from $TH^+$ cells to the neighboring glial cells (co-localizing with the glial marker GFAP, Figure 3E).

## Changes in $CO_2$ Significantly Modifies the Excitability of Neurons in the VTA

During the CBF loading assay carried out in the P17–21 slices, although no dye-filled neurons were observed in the SN, unexpectedly a population of dye-filled neurons was observed in the neighboring VTA (Figure 4A). This region is central to circuits controlling motivation, reward, and goal-directed behaviors (Morales and Margolis,

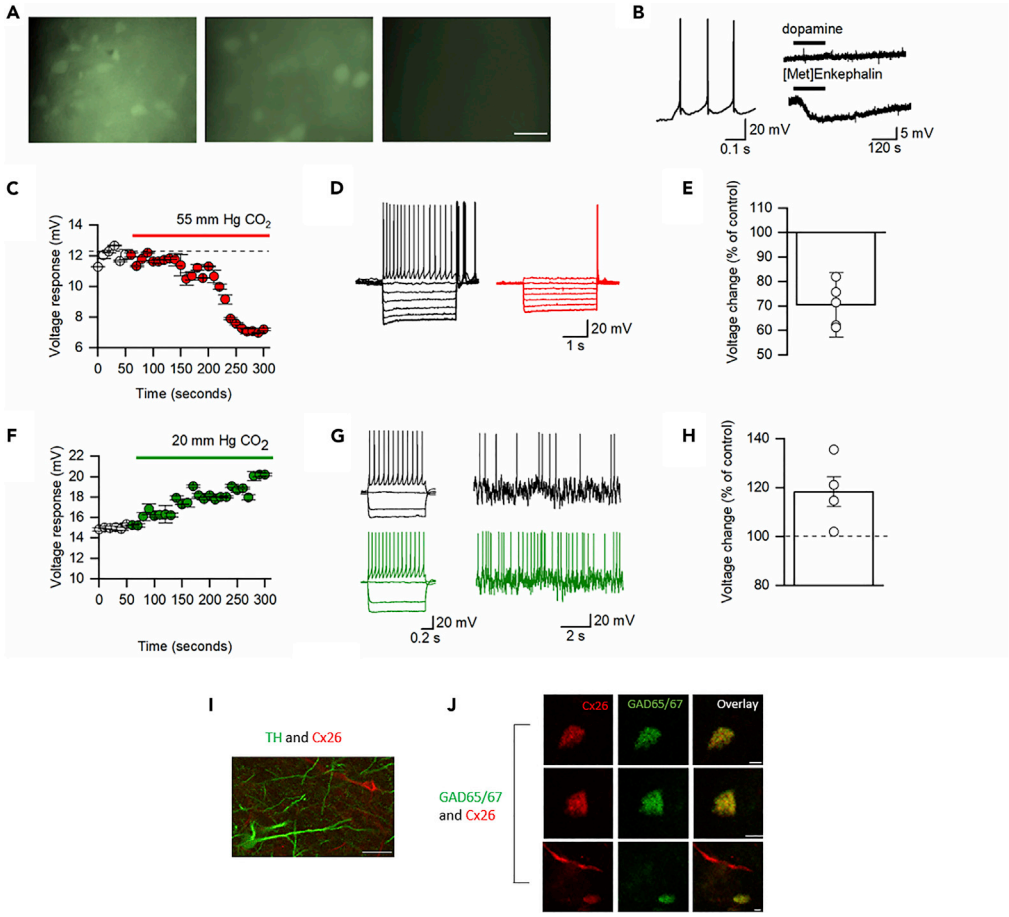


**Figure 4. GABAergic Neurons in the VTA Are Sensitive to $CO_2$**

(A) CBF dye loading of VTA neurons in response to hypercapnia occurs at both P7–10 and P17–21 but does not occur without the increase in $CO_2$ (hypercapnia), scale bar, 50 μM.

(B) Characteristics of $CO_2$-sensitive VTA neurons: firing pattern, hyperpolarization to the opioid receptor agonist [Met5] Enkephalin (10 μM) but not to dopamine (30 μM).

(C) Time course of changes in voltage response ($CO_2$ increased from 35 to 55 mm Hg, each point is a mean of six current steps, error bars are SEM).

(D) Voltage responses to step currents at indicated time points in (C).

(E) Quantification of changes in voltage response to increased $CO_2$.

(F) Time course of changes in voltage response ($CO_2$ decreased from 35 to 20 mm Hg, each point is a mean of six current steps, error bars are SEM).

(G) Voltage responses to step and fluctuating current inputs (as in Badel et al., 2008; see Methods) at indicated time points in (F) demonstrating increased input resistance and firing rate.

(H) Quantification of changes in voltage response to decreased $CO_2$.

(I and J) Representative single optical planes immunohistochemistry images. (I) Immunofluorescent staining of P17–21 VTA for Cx26 (red), which is not expressed by $TH^+$ neurons (green, no co-localization); scale bar, 50 μM. (J) Co-localization of Cx26 (red) with the soma of three individual $GAD^+$ neurons (green) in the VTA (scale bar, 20 μM).

2017). Dye-loaded neurons in the VTA had a markedly different firing pattern and voltage response to current injection compared with SN DNs, were not hyperpolarized by dopamine, but were hyperpolarized by the opioid receptor agonist [Met5]Enkephalin, therefore, they could instead be GABAergic neurons (Johnson and North, 1992; Figure 4B). These VTA neurons showed electrophysiological changes similar to that observed for P7–10 SN DNs in response to changes in $PCO_2$: increased $PCO_2$ (55 mm Hg) decreased input resistance (voltage response reduced to 71 ± 13.2% of control $p = 0.0055$, 335 ± 66.7 to 222 ± 39.4 MΩ, $p = 0.0446$, before the sag $n = 5$) and firing rate (Figures 4C–4E). Reducing $PCO_2$ to 20 mm Hg increased input resistance (voltage response increased to 118 ± 6.1%, $p = 0.0428$) and firing rate (193 ± 35%, $p = 0.049$, of control, Figures 4F–4H). To identify the phenotype of the $CO_2$-sensitive neurons in the VTA, we carried out

immunohistochemistry. Cx26 was not expressed in $TH^+$ neurons in the VTA, so is not present in dopaminergic neurons (Figure 3I). However, Cx26 immunoreactivity was present in $GAD65/67^+$ neurons (Figure 3J), a marker for GABAergic neurons in the VTA (Chieng et al., 2011), which fits with the electrophysiological properties of the $CO_2$-sensitive neurons. Thus, the $CO_2$-sensitive neurons in the VTA are GABAergic.

## DISCUSSION

We have demonstrated an unexpected $CO_2$-sensitive phenotype for neurons in the SN at P7–10 and in the VTA, with increases in $CO_2$ markedly increasing their resting conductance. This effect appears to occur in only specific subtypes of neuron, as for example, it was not observed in hippocampal pyramidal cells. It is well established that increases in $PCO_2$ can close gap junctions and that DN neurons in young animals are coupled (Connors et al., 1984; Bukauskas and Peracchia, 1997; Vandecasteele, 2005). However, this effect cannot account for the effects that we have observed. First, the increase in $PCO_2$ that is required to close gap junctions is large and is well above the range of $PCO_2$ changes we used to elicit effects on neuron electrophysiology. In addition, the closure of gap junctions would result in a decrease in whole-cell conductance and an increase in excitability, which is the opposite of what we observed in our study. Here we have provided several lines of evidence that suggest that our observations of an increase in $CO_2$-sensitive conductance result from the opening of Cx26 hemichannels, whose open probability increases through the direct $CO_2$-mediated carbamylation of lysine residues (Meigh et al., 2013). We have shown that the effects of $CO_2$ in SN DNs occurs over the same developmental period as they express Cx26 mRNA (measured in an independent study, Vandecasteele et al., 2006). The effects of increasing $PCO_2$ on resting conductance can be blocked by the hemichannel inhibitor carbenoxolone. Although carbenoxolone has neuronal and synaptic effects as well as blocking hemichannels, they would be expected to accentuate the observed increase in conductance rather than reducing it, therefore not obscuring the observations (Tovar et al., 2009). If the effects of $PCO_2$ on cell conductance are due to the opening of Cx26 hemichannels, it would be predicted that, since the midpoint of Cx26 hemichannel opening lies around the basal level of $PCO_2$ in our experiments (Meigh et al., 2013, 35 mM Hg), a decrease in $CO_2$ would close Cx26 hemichannels leading to a decrease in the resting conductance. Such a decrease in conductance could be observed for both SN DN and VTA GABAergic neurons when $CO_2$ was lowered.

SN dopaminergic neurons and VTA GABAergic neurons could be filled with a membrane-impermeant fluorescent dye (CBF) when $PCO_2$ was increased (dye loading). CBF will pass through Cx26 hemichannels when they are open and then become trapped inside cells when the hemichannels are subsequently closed (Huckstepp et al., 2010a; Meigh et al., 2013). Unfortunately, CBF cannot be fixed with paraformaldehyde, which prevents the dye-filled neurons from being subsequently labeled using immunohistochemistry. However, we can be confident that the dye-filled cells were either SN DNs or VTA GABAergic neurons, as patch clamp recording was carried out before the dye loading (to confirm the identity of the cells from their electrophysiological properties and pharmacology) and then the same cells were subsequently dye filled. We have also used immunohistochemistry to show that Cx26 protein is expressed in these neurons. The expression pattern of Cx26 across development in SN DNs matched that reported for Cx26 mRNA expression (Vandecasteele et al., 2006). This particular Cx26 antibody (13-8100) has been used extensively to study the role of Cx26 in breathing. There are many independent papers that demonstrate the specificity of this antibody in KO of Cx26. KO of Cx26 in the organ of Corti abolishes Cx26 immunoreactivity with this antibody (Sun et al., 2009), and our prior publications show correspondence for Cx26 immunostaining with a reporter driven from the endogenous Cx26 promoter (Huckstepp et al., 2010a, 2010b).

To separate the effects of $CO_2$ from any effects of changing pH, we kept extracellular pH constant during our experiments by using isohydric solutions (an increase in $PCO_2$ under these conditions is termed isohydric hypercapnia). However, we did not measure intracellular pH and there will probably be transient changes in pH when the solutions are exchanged. It is well documented that intracellular pH will transiently acidify on application of the stimulus (raised $PCO_2$) and transiently alkalinize on its removal (Filosa et al., 2002; Putnam, 2001). A mild intracellular acidification would be expected to result in hemichannel closure and therefore a decrease in conductance. Therefore, we concluded that our observations were not the result of a change in intracellular pH. In addition, these transient changes in pH cannot explain the marked and sustained changes in conductance that only occur in these specific subtypes of neuron.

In this paper we have outlined the $CO_2$ sensitivity of specific neurons in the SN and VTA and provided a mechanism for this effect: Cx26 hemichannel expression. As far as we are aware this is the first documentation of neuronal expression of Cx26, which is usually found in glia (Nagy et al., 2011). Although we have carried

out no behavioral analysis of the effects of $CO_2$ sensitivity, it is interesting to speculate on its possible behavioral consequences. Since the mid-point of Cx26 opening lies around the resting level of $CO_2$ in humans (Huckstepp et al., 2010a, 2010b; Meigh et al., 2013), small increases or decreases in $CO_2$ will modulate neuron excitability and thus could potentially modulate behavior. This $CO_2$ sensitivity switches from SN neurons to glia during early postnatal development but is retained in GABAergic neurons in the VTA. The switch from neuronal to glial expression could change the signaling direction from inhibitory to excitatory, as opening hemichannels in glia can allow the diffusion of molecules such as ATP, which could in turn excite SN DNs (through P2X or P2Y receptor activation). One speculated role for the $CO_2$-mediated reduction in excitability of SN DNs in early postnatal life is, since the nest is likely to be hypercapnic, inhibition of movement may promote suckling behavior. The maintenance of $CO_2$ sensitivity in the VTA postnatally is particularly interesting given its role in reward, addiction, motivation (Volkow and Morales, 2015), and sleep-wake behaviors (Eban-Rothschild et al., 2016). Activation of GABAergic neurons in the VTA induces sleep, and their inhibition increases wakefulness (Yu et al., 2018). There are several contributing mechanisms to hypercapnic arousal. The orexinergic neurons of the lateral hypothalamus, known to promote wakefulness, can be activated by hypercapnia, although this is through a pH-dependent transduction mechanism (Williams et al., 2007). The histaminergic neurons of the tuberomamillary nucleus (TMN), which also promote wakefulness, are activated by $CO_2$ (Johnson et al., 2005; Anaclet et al., 2009). Neurons of the dorsal raphe, not involved in the control of breathing are pH/$CO_2$ sensitive and contribute to hypercapnic arousal (Smith et al., 2018). Furthermore, the parabrachial nucleus integrates chemosensory inputs during hypercapnia from the medullary nuclei such as the retrotrapezoid nucleus and the raphe magnus, which contain pH-sensitive neurons to mediate arousal (Kaur et al., 2017). However, even after silencing these key relay neurons, hypercapnia still results in arousal albeit at a longer latency showing that other parallel pathways are involved (Kaur et al., 2017). Given that inhibition of the VTA GABAergic neurons have been demonstrated to cause wakefulness (Yu et al., 2018) we hypothesize that inhibition of these neurons by modestly raised $CO_2$ could potentially contribute an additional parallel pathway of hypercapnic arousal.

### Limitations of the Study

This report outlines the novel observation of $CO_2$ sensitivity in a specific subset of neurons with several lines of evidence that it results from Cx26 hemichannel expression. There is no data on the physiological significance of this $CO_2$ sensitivity, in particular regarding movement and reward behavior. This will be examined in future studies. There is no quantification of the expression pattern of Cx26 protein in either $TH^+$ or $GAD^+$ neurons. In the future, tools like fluorescence in situ hybridization (FISH) could be used to produce more accurate measurements of expression.

### Resource Availability

#### *Lead Contact*

Further information and requests for resources and reagents should be directed to and will be fulfilled by Mark Wall (Mark.Wall@warwick.ac.uk) or Emily Hill (E.hill.2@warwick.ac.uk).

#### *Materials Availability*

This study did not generate new unique reagents.

#### *Data and Code Availability*

This study did not generate new code or structural datasets.

## METHODS

All methods can be found in the accompanying Transparent Methods supplemental file.

## SUPPLEMENTAL INFORMATION

Supplemental Information can be found online at https://doi.org/10.1016/j.isci.2020.101343.

## ACKNOWLEDGMENTS

This work was supported by a Biotechnology and Biological Sciences Research Council-funded doctoral fellowship (E.H.) We would like to thank Dr. Huckstepp, Dr. Bhandare, and Dr. van de Wiel for their technical assistance.

## AUTHOR CONTRIBUTIONS

E.H., M.J.W., and N.D. designed the experiments. E.H. conducted the experiments and performed the analysis. E.H., M.J.W., and N.D. wrote the manuscript.

## DECLARATION OF INTERESTS

The authors declare no competing interests.

Received: March 9, 2020
Revised: April 30, 2020
Accepted: July 1, 2020
Published: July 24, 2020

## REFERENCES

Anaclet, C., Parmentier, R., Ouk, K., Guidon, G., Buda, C., Sastre, J.P., Akaoka, H., Sergeeva, O.A., Yanagisawa, M., Ohtsu, H., et al. (2009). Orexin/hypocretin and histamine: distinct roles in the control of wakefulness demonstrated using knock-out mouse models. J. Neurosci. *29*, 14423–14438.

Badel, L., Lefort, S., Brette, Petersen, C.C.H., Gerstner, W., and Richardson, M.J.E. (2008). Dynamic I-V curves are reliable predictors of naturalistic pyramidal-neuron voltage traces. J. Neurophysiol. *99*, 656–666.

Bukauskas, F., and Peracchia, C. (1997). Two distinct gating mechanisms in gap junction channels: CO2-sensitive and voltage-sensitive. Biophysical J. *72*, 2137–2142.

Chieng, B., Azriel, Y., Mohammadi, S., and Christie, M. (2011). Distinct cellular properties of identified dopaminergic and GABAergic neurons in the mouse ventral tegmental area. J. Physiol. *589*, 3775–3787.

Connors, B., Benardo, L., and Prince, D. (1984). Carbon dioxide sensitivity of dye coupling among glia and neurons of the neocortex. J. Neurosci. *4*, 1324–1330.

Dufour, M., Woodhouse, A., Amendola, J., and Goaillard, J. (2014). Non-linear developmental trajectory of electrical phenotype in rat substantia nigra pars compacta dopaminergic neurons. Elife *3*, e04059.

Eban-Rothschild, A., Rothschild, G., Giardino, W., Jones, J., and de Lecea, L. (2016). Neuronal mechanisms for sleep/wake regulation and modulatory drive. Nat. Neurosci. *19*, 1356–1366.

Eldridge, F.L., Kiley, J.P., and Millhorn, D.E. (1985). Respiratory responses to medullary hydrogen ion changes in cats: different effects of respiratory and metabolic acidoses. J. Physiol. *358*, 285–297.

Filosa, J.A., Dean, J.B., and Putnam, R.W. (2002). Role of intracellular and extracellular pH in the chemosensitive response of rat locus coeruleus neurones. J. Physiol. *541*, 493–509.

Gourine, A.V., Kasymov, V., Marina, N., Tang, F., Figueiredo, M.F., Lane, S., Teschemacher, A.G., Spyer, K.M., Deisseroth, K., and Kasparov, S. (2010). Astrocytes control breathing through pH-dependent release of ATP. Science *329*, 571–575.

Gourine, A.V., Llaudet, E., Dale, N., and Spyer, K.M. (2005). ATP is a mediator of chemosensory transduction in the central nervous system. Nature *436*, 108–111.

Grace, A., and Bunney, B. (1983). Intracellular and extracellular electrophysiology of nigral dopaminergic neurons—3. Evidence for electrotonic coupling. Neuroscience *10*, 333–348.

Grace, A., and Onn, S. (1989). Morphology and electrophysiological properties of immunocytochemically identified rat dopamine neurons recorded in vitro. J. Neurosci. *9*, 3463–3481.

Hosford, P.S., Mosienko, V., Kishi, K., Jurisic, G., Seuwen, K., Kinzel, B., Ludwig, M.G., Wells, J.A., Christie, I.N., Koolen, L., et al. (2018). CNS distribution, signalling properties and central effects of G-protein coupled receptor 4. Neuropharmacology *138*, 381–392.

Huckstepp, R.T., Eason, R., Sachdev, A., and Dale, N. (2010a). CO2-dependent opening of connexin 26 and related beta connexins. J. Physiol. *588*, 3921–3931.

Huckstepp, R.T., id Bihi, R., Eason, R., Spyer, K.M., Dicke, N., Willecke, K., Marina, N., Gourine, A.V., and Dale, N. (2010b). Connexin hemichannel-mediated CO2-dependent release of ATP in the medulla oblongata contributes to central respiratory chemosensitivity. J. Physiol. *588*, 3901–3920.

Johnson, P.L., Moratalla, R., Lightman, S.L., and Lowry, C.A. (2005). Are tuberomammillary histaminergic neurons involved in CO2-mediated arousal? Exp. Neurol. *193*, 228–233.

Johnson, S., and North, R. (1992). Two types of neurone in the rat ventral tegmental area and their synaptic inputs. J. Physiol. *450*, 455–468.

Kaur, S., Wang, J., Ferrari, L., Thankachan, S., Kroeger, D., Venner, A., Lazarus, M., Wellman, A., Arrigoni, E., Fuller, P., and Saper, C. (2017). A genetically defined circuit for arousal from sleep during hypercapnia. Neuron *96*, 1153–1167.e5.

kumar, N.N., Velic, A., Soliz, J., Shi, Y., Li, K., Wang, S., Weaver, J.L., Sen, J., Abbott, S.B., Lazarenko, R.M., et al. (2015). Regulation of breathing by CO(2) requires the proton-activated receptor GPR4 in retrotrapezoid nucleus neurons. Science *348*, 1255–1260.

Loeschcke, H. (1982). Central chemosensitivity and the reaction theory. J. Physiol. *332*, 1–24.

Meigh, L., Greenhalgh, S.A., Rodgers, T.L., Cann, M.J., Roper, D.I., and Dale, N. (2013). CO2 directly modulates connexin 26 by formation of carbamate bridges between subunits. Elife *2*, e01213.

Morales, M., and Margolis, E. (2017). Ventral tegmental area: cellular heterogeneity, connectivity and behaviour. Nat. Rev. Neurosci. *18*, 73–85.

Nagy, J., Lynn, B., Tress, O., Willecke, K., and Rash, J. (2011). Connexin26 expression in brain parenchymal cells demonstrated by targeted connexin ablation in transgenic mice. Eur. J. Neurosci. *34*, 263–271.

Neuhoff, H., Neu, A., Liss, B., and Roeper, J. (2002). Ih channels contribute to the different functional properties of identified dopaminergic subpopulations in the midbrain. J. Neurosci. *22*, 1290–1302.

Putnam, R.W. (2001). Intracellular pH regulation of neurons in chemosensitive and nonchemosensitive areas of brain slices. Respir. Physiol. *129*, 37–56.

Shams, H. (1985). Differential effects of CO2 and H+ as central stimuli of respiration in the cat. J. Appl. Physiol. *58*, 357–364.

Smith, H.R., Leibold, N.K., Rappoport, D.A., Ginapp, C.M., Purnell, B.S., Bode, N.M., Alberico, S.L., Kim, Y.C., Audero, E., Gross, C.T., and Buchanan, G.F. (2018). Dorsal raphe serotonin neurons mediate CO2-induced arousal from sleep. J. Neurosci. *38*, 1915–1925.

Sun, Y., Tang, W., Chang, Q., Wang, Y., Kong, W., and Lin, X. (2009). Connexin30 null and conditional connexin26 null mice display distinct pattern and time course of cellular degeneration in the cochlea. J. Comp. Neurol. *516*, 569–579.

Tovar, K., Maher, B., and Westbrook, G. (2009). Direct actions of carbenoxolone on synaptic transmission and neuronal membrane properties. J. Neurophysiol. *102*, 974–978.

Trapp, S., Aller, M.I., Wisden, W., and Gourine, A.V. (2008). A role for TASK-1 (KCNK3) channels in the chemosensory control of breathing. J. Neurosci. *28*, 8844–8850.

Turovsky, E., Theparambil, S.M., Kasymov, V., Deitmer, J.W., Del Arroyo, A.G., Ackland, G.L., Corneveaux, J.J., Allen, A.N., Huentelman, M.J., Kasparov, S., et al. (2016). Mechanisms of CO2/H+ sensitivity of astrocytes. J. Neurosci. *36*, 10750–10758.

van de Wiel, J., Meigh, L., Bhandare, A., Cook, J., Huckstepp, R.T., and Dale, N. (2020). Connexin26 mediates CO2-dependent regulation of breathing via glial cells of the medulla oblongata. bioRxiv. https://doi.org/10.1101/2020.04.16.042440.

Vandecasteele, M. (2005). Electrical synapses between dopaminergic neurons of the substantia nigra pars compacta. J. Neurosci. *25*, 291–298.

Vandecasteele, M., Glowinski, J., and Venance, L. (2006). Connexin mRNA expression in single dopaminergic neurons of substantia nigra pars compacta. Neurosci. Res. *56*, 419–426.

Volkow, N., and Morales, M. (2015). the brain on drugs: from reward to addiction. Cell *162*, 712–725.

Wang, S., Benamer, N., Zanella, S., Kumar, N.N., Shi, Y., Bevengut, M., Penton, D., Guyenet, P.G., Lesage, F., Gestreau, C., et al. (2013). TASK-2 channels contribute to pH sensitivity of retrotrapezoid nucleus chemoreceptor neurons. J. Neurosci. *33*, 16033–16044.

Wenker, I.C., Sobrinho, C.R., Takakura, A.C., Moreira, T.S., and Mulkey, D.K. (2012). Regulation of ventral surface CO2/H+-sensitive neurons by purinergic signalling. J. Physiol. *590*, 2137–2150.

Williams, R.H., Jensen, L.T., Verkhratsky, A., Fugger, L., and Burdakov, D. (2007). Control of hypothalamic orexin neurons by acid and CO2. Proc. Natl. Acad. Sci. U S A *104*, 10685–10690.

Yu, X., Li, W., Ma, Y., Tossell, K., Harris, J., Harding, E., Ba, W., Miracca, G., Wang, D., Li, L., et al. (2018). GABA and glutamate neurons in the VTA regulate sleep and wakefulness. Nat. Neurosci. *22*, 106–119.

**iScience, Volume *23***

## Supplemental Information

# Moderate Changes in $CO_2$ Modulate the Firing of Neurons in the VTA and Substantia Nigra

**Emily Hill, Nicholas Dale, and Mark J. Wall**

**Supplementary Data**

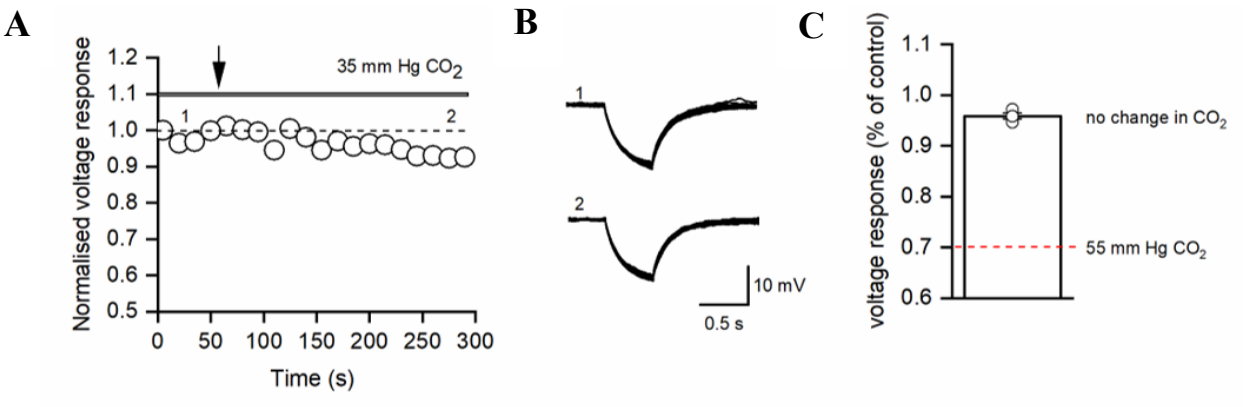


**Figure S1. Control for stability of recordings and for changing solution but maintaining constant $PCO_2$, related to figure 1.** (A) Graph plotting the voltage response to 50 pA hyperpolarising current steps from a P10 SN DN with each point the mean of 15 sweeps. The $CO_2$ was maintained at 35 mm Hg but solutions were exchanged (arrow) to ensure that the observations are not an artefact of the solution switching process. This also illustrates the stability of voltage responses throughout the recording. (B) Associated voltage traces (50 superimposed traces) in response to step currents at the indicated time points from A. (C) Quantification of the voltage response changes when the solution was exchanged, relative to the amplitude of the response at whole cell breakthrough, data is presented as mean ± SEM (points are from individual experiments). Red dashed line represents the decrease in response for cells which were exposed to high $CO_2$ (55 mm Hg) after an equal amount of time. There is no effect of changing solution and the voltage response is stable over the duration of the recording.

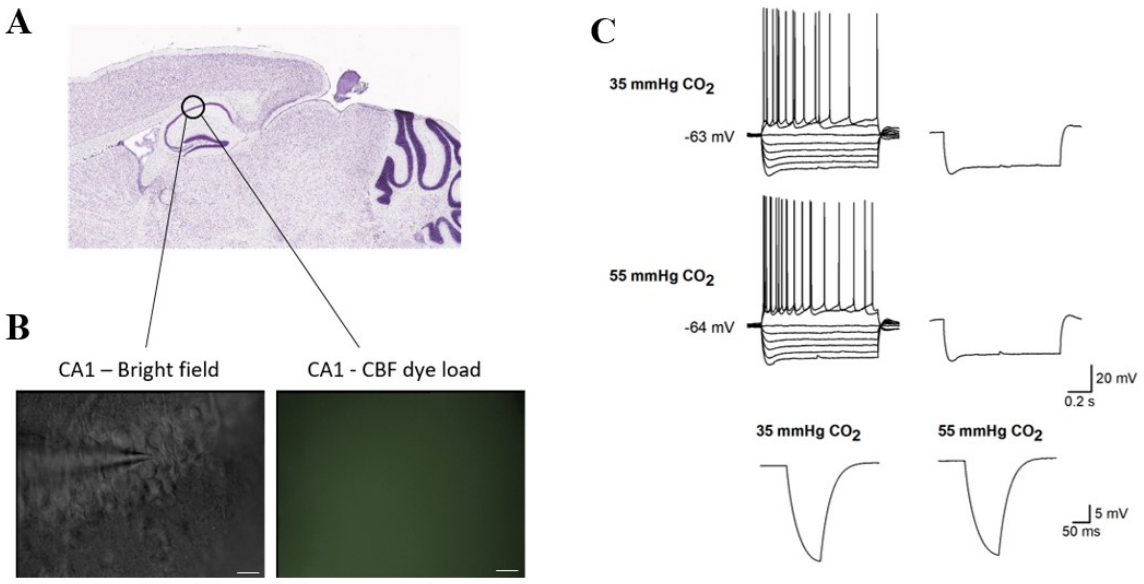


**Figure S2: CA1 pyramidal cells show no dye loading or electrophysiological changes in response to high $CO_2$, related to figure 1** (A) Localisation of CA1 region of the hippocampus in a sagittal slice (Adapted from Allen Mouse Brain Atlas, 2004). (B), (left) Bright-field image of the CA1 region demonstrating the location of a recorded pyramidal cell (scale bar = 30 μM). The slice was then subjected to carboxy-fluorescein (CBF) dye-loading (see methods) as used for the SN and VTA. There was no visible dye loading of the neurons (right). (C), (Top) Membrane potential traces recorded from a CA1 pyramidal neuron in response to current steps (3 s steps starting at -200 pA, increasing by 50 pA until there is a regular firing pattern) in 35 mmHg $CO_2$. (Inset) Single membrane potential trace in response to the injection of -200 pA (3 s) in 35 mmHg $CO_2$. (Bottom) Membrane potential traces recorded from the same CA1 pyramidal neuron in response to current steps in 55 mmHg $CO_2$. Single membrane potential trace in response to a -200 pA (3 s) current step in 55 mmHg $CO_2$.

**Table S1: Comparison of the electrophysiological parameters of P7-10 and P17-21 SN dopaminergic neurons, related to figure 1.**

| | Rin (pre-sag) MΩ | | | Rin Steady MΩ | | | RMP | | |
|---|---|---|---|---|---|---|---|---|---|
| | **Mean** | **SEM** | **95% CI** | **Mean** | **SEM** | **95% CI** | **Mean** | **SEM** | **95% CI** |
| **P7-10** | 380.4 | ± 28.16 | ± 55.2 | 246.9 | ± 24.63 | ± 48.3 | -59.3 | ± 1.33 | ± 2.6 |
| **P17-21** | 289.8 | ± 22.45 | ± 44 | 193.9 | ± 42.85 | ± 84 | -60 | ± 2.08 | ± 4.07 |

Rin Steady: Mann-Whitney non parametric test p = 0.3037 ns

Rin Pre Sag: Mann-Whitney non parametric test: p = 0.0977 ns

RMP: Mann- Whitney non parametric test p = 0.8352 ns

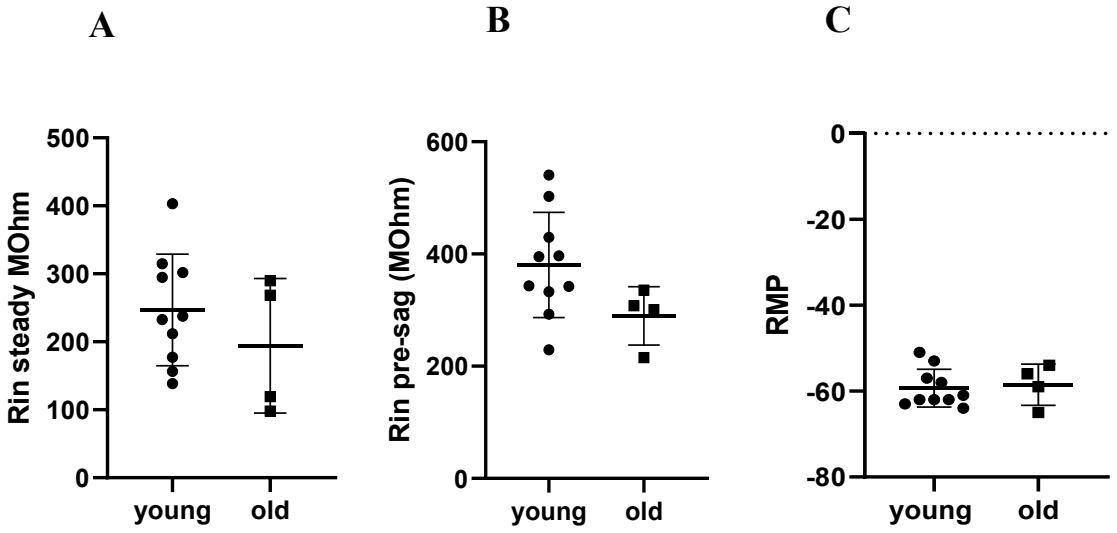


**Figure S3: Comparison of the electrophysiological parameters of P7-10 and P17-21 SN neurons, related to figure 1.**

Input resistance measurements 'both before the sag' (A) and at 'steady state' (B) decreased during development in line with published studies (4). We saw no difference in the stability of recordings and there was no change to resting membrane potential (C).

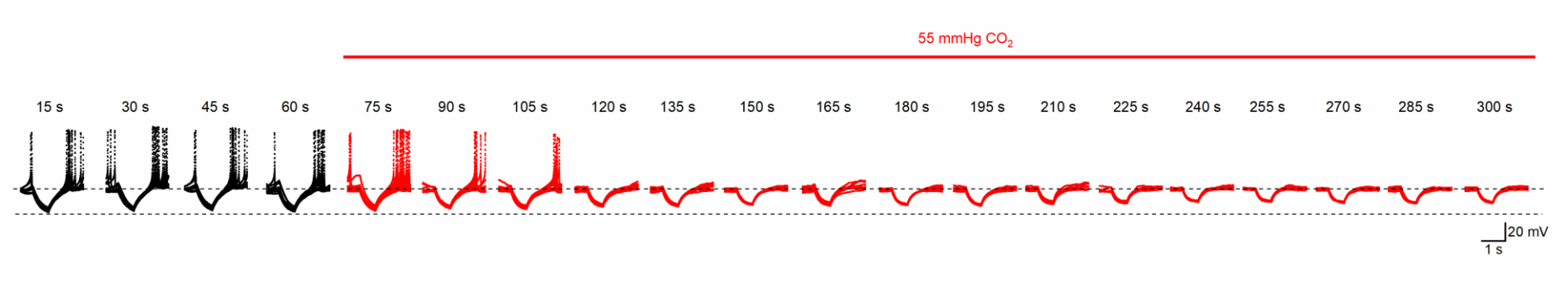


**Figure S4: Example raw data traces for the full timeframe of raised $CO_2$ exposure, related to figure 1.** A representative example from a P7-10 substantia nigra dopaminergic neuron. Membrane potential traces in response to -50 pA current steps in 35 mmHg $CO_2$ (black), then switched over to 55 mmHg $CO_2$ (red). Each plot represents a timepoint from the graph in Figure 1B and displays 9 overlaid sweeps within each 15 second time interval. A clear reduction in voltage response can be observed over time, as is summarised in Figure 1B-C.

**Raw data plots**

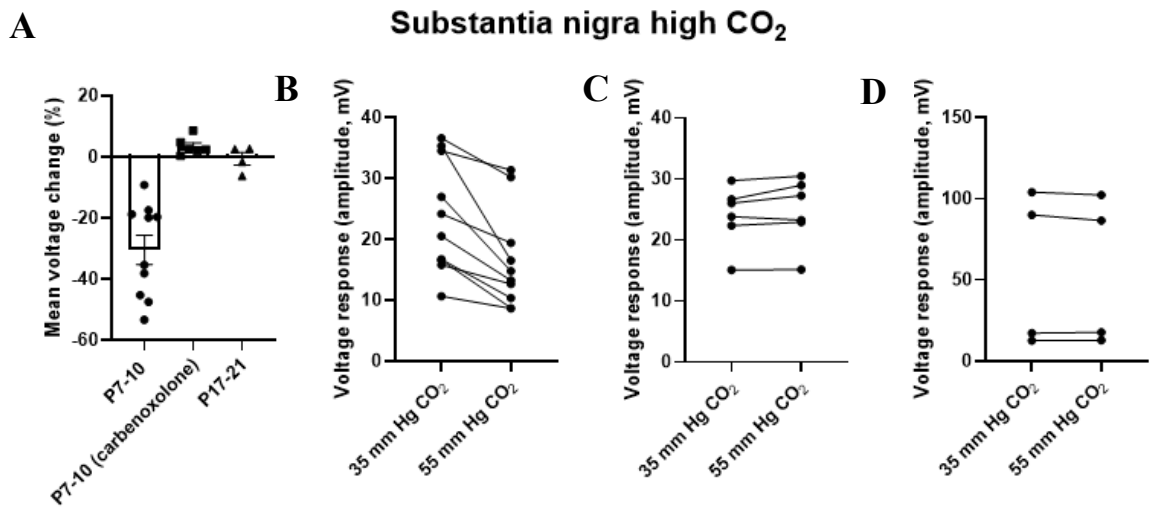


**Figure S5: Raw data plots for raising $CO_2$ in the substantia nigra, related to figure 1** Quantification of voltage response changes (35 to 55 mm Hg $CO_2$), replicated from 1I. B-D represent the amplitude of the voltage response to a 50-pA hyperpolarising step current injection, in 35 mm Hg $CO_2$ and 55 mm Hg $CO_2$. Data points from each experiment is joined up by a line to represent that they are paired. It can be clearly observed in (B) that there is a decrease in the amplitude of the voltage response for P7-10 mice, which is not replicated in the presence of carbenoxolone (C) or in older mice (P17-21, D).

**Table S2: Statistical analysis of data on raising $CO_2$ in the substantia nigra, related to figure 1**

| | |
|---|---|
| SN P7-10, 35 mm Hg **vs** 55 mm Hg | p=0.0020 |
| SN P7-10 (carbenoxolone), 35 mm Hg **vs** 55 mm Hg | p=0.0938 |
| SN P17-21, 35 mm Hg **vs** 55 mm Hg | p=0.3302 |
| **Kruskal-Wallis ANOVA:** | p<0.0001 |
| SN P7-10 **vs** P7-10 (carbenoxolone) **vs** P17-21 | |
| **Dunn's multiple comparisons:** | p=0.0014 |
| P7-10 **vs** P7-10 (carbenoxolone) | p=0.0304 |
| P7-10 **vs** P17-21 | p>0.9999 |
| P7-10 (carbenoxolone) **vs** P17-21 | |

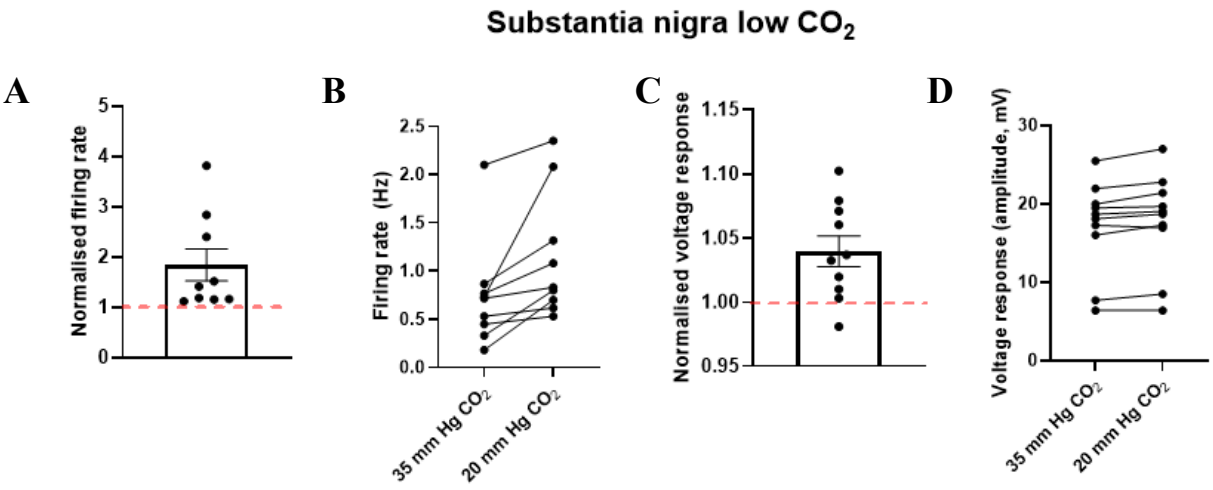


**Figure 6: Raw data plots for lowering $CO_2$ in the substantia nigra, related to figure 2.** A. Quantification of the firing rate changes (35 mm Hg to 20 mm Hg $CO_2$), replicated from 2D. B. Raw firing rate data, in 35 mm Hg $CO_2$ and 20 mm Hg $CO_2$. C. Quantification of voltage response changes (35 to 20 mm Hg $CO_2$), replicated from 2E. D. The amplitude of the voltage response to a 50-pA hyperpolarising step current injection, in 35 mm Hg $CO_2$ and 20 mm Hg $CO_2$. In B and D, data points from each experiment is joined up by a line to represent that they are paired. An increase in firing rate and voltage response are observed.

**Table S3: Statistical analysis of data on lowering $CO_2$ in the substantia nigra, related to figure 2**

| | |
|---|---|
| SN Firing rate, 35 mm Hg **vs** 20 mm Hg | p=0.0039 |
| SN Voltage response 35 mm Hg **vs** 20 mm Hg | p=0.0098 |

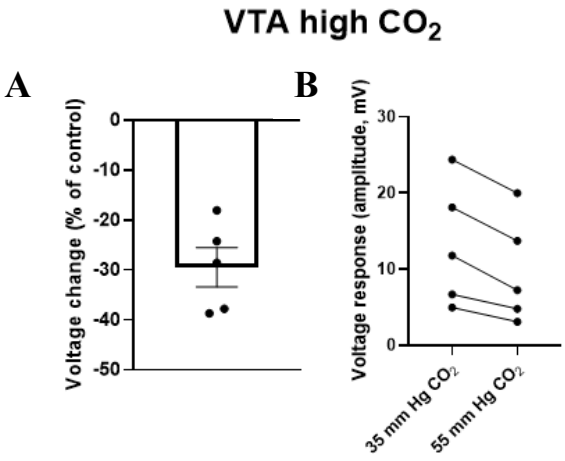


**Figure S7: Raw data plots for raising $CO_2$ in the ventral tegmental area, related to figure 4.** A. Quantification of voltage response changes (35 to 55 mm Hg $CO_2$), replicated from 3E. B. The amplitude of the voltage response to a 50-pA hyperpolarising step current injection, in 35 mm Hg $CO_2$ and 55 mm Hg $CO_2$. Data points from each experiment is joined up by a line to represent that they are paired. A decrease in voltage response can be observed.

**Table S4: Statistical analysis of the data on raising $CO_2$ in the ventral tegmental area, related to figure 4**

| | |
|---|---|
| VTA Voltage response 35 mm Hg **vs** 55 mm Hg | p=0.0055 |

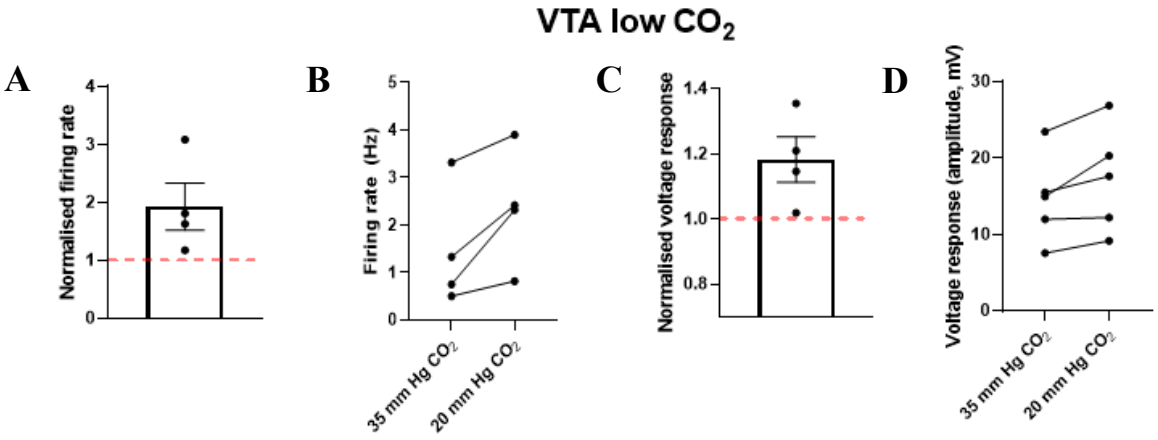


**Figure S8: Raw data plots for lowering $CO_2$ in the ventral tegmental area, related to figure 4** A. Quantification of the firing rate changes (35 mm Hg to 20 mm Hg $CO_2$). B. Raw firing rate data, in 35 mm Hg $CO_2$ and 20 mm Hg $CO_2$. C. Quantification of voltage response changes (35 to 20 mm Hg $CO_2$), replicated from 3H. D. The amplitude of the voltage response to a 50-pA hyperpolarising step current injection, in 35 mm Hg $CO_2$ and 20 mm Hg $CO_2$. In B and D, data points from each experiment is joined up by a line to represent that they are paired. An increase in firing rate and voltage response are observed. Increases to both firing rate and voltage response can be observed.

**Table S5: Statistical analysis of the data on lowering $CO_2$ in the ventral tegmental area, related to figure 4**

| | |
|---|---|
| VTA Voltage response 35 mm Hg **vs** 55 mm Hg | p=0.0428 |
| VTA Firing Rate 35 mm Hg **vs** 55 mm Hg | p=0.0490 |

## Transparent methods

### KEY RESOURCES TABLE

| REAGENT or RESOURCE | SOURCE | IDENTIFIER |
|---|---|---|
| **Antibodies** | | |
| Sheep polyclonal Anti-Tyrosine hydroxylase | Merck | AB1542 |
| Mouse monoclonal anti-Connexin 26 | Invitrogen | 138100 |
| Chicken polyclonal anti-GFAP | Abcam | ab4674 |
| Rabbit polyclonal anti-GAD65 + GAD67 | Abcam | ab49832 |
| Donkey anti-sheep 594 | Invitrogen | A11016 |
| Donkey anti-mouse 594 | Invitrogen | A21203 |
| Donkey anti-sheep 488 | Invitrogen | A11015 |
| Goat anti-chicken 488 | Invitrogen | A11039 |
| Goat anti-Rabbit 488 | Invitrogen | A11008 |
| **Chemicals, Peptides, and Recombinant Proteins** | | |
| Met5[enkephalin] | Merck | M6638 |
| Carbenoxolone disodium salt | Sigma Aldrich | C4790-1G |
| Dopamine Hydrochloride | Sigma Aldrich | H8502-5G |
| (6)-Carboxy-fluorescein (CBF) | Novabiochem | 8.51082.001 |
| Alexa Fluor 594 hydrazide | Molecular Probes | 10072752 |
| **Software and Algorithms** | | |
| pClamp | http://www.moleculardevices.com/products/software/pclamp.html | RRID:SCR_011323 |
| Zen Black | http://www.zeiss.com/microscopy/en_us/products/microscope-software/zen.html#introduction | RRID:SCR_013672 |
| Origin | http://www.originlab.com/index.aspx?go=PRODUCTS/Origin | RRID:SCR_014212 |

## Methods

### Preparation of acute brain slices

All experiments were approved by the local Animals Welfare and Ethics Board (AWERB) at the University of Warwick. C57/Bl6 mice from two age groups (P7-10 and P17-21) were killed by cervical dislocation and decapitated in accordance with the U.K. Animals (Scientific Procedures) Act (1986). The brain was rapidly dissected and kept on ice. The cerebellum was removed, and the rostral section of the brain was trimmed. The brain was then mounted rostral side down. Coronal slices (350 μM) were cut with a Microm HM 650V microslicer in cold (2-4°C) high $Mg^{2+}$, low $Ca^{2+}$ aCSF, composed of (mM): 127 NaCl, 1.9 KCl, 8 $MgCl_2$, 0.5 $CaCl_2$, 1.2 $KH_2PO_4$, 26 $NaHCO_3$, 10 D-glucose (pH 7.4 when bubbled with 95% $O_2$ and 5% $CO_2$, 300 mOSM). Slices were stored at 34 °C in standard aCSF (1 mM $Mg^{2+}$ and 2 mM $Ca^{2+}$) for 1 to 8 hours.

### Whole-cell patch clamp recording

A slice was transferred to the recording chamber, submerged and perfused (2-3 ml/$min^{-1}$) with aCSF at 30 °C. Slices were visualized using IR-DIC optics with an Olympus BX151W microscope (Scientifica, Bedford UK) and a CCD camera (Hitachi). Whole-cell current-clamp recordings were made from neurons in the substantia nigra, ventral tegmental area or from CA1 pyramidal neurons in the hippocampus using patch pipettes (5–10 MΩ) manufactured from thick walled glass (Harvard Apparatus, Edenbridge, UK). Intracellular solution was filtered before use (0.2 μm) and contained in (mM): potassium gluconate 135, NaCl 7, HEPES 10, EGTA 0.5, phosphocreatine 10, MgATP 2, NaGTP 0.3 293 mOSM, pH 7.2). A subset of neurons were filled with AF594 dye (50 μM) via the patch pipette for immunohistochemistry. Voltage recordings were made using an Axon Multiclamp 700B amplifier

(Molecular Devices, USA) and digitised at 20 KHz. Data acquisition and analysis were performed using pClamp 10 (Molecular Devices). Recordings from neurons that had a resting membrane potential of between -55 and – 75 mV at whole-cell breakthrough were accepted for analysis. The bridge balance was monitored throughout the experiments and any recordings where it changed by more than 20 % were discarded.

**Solutions are based on Huckstepp et al (2010)**

**Control (35 mmHg $CO_2$) aCSF contained in (mM):** NaCl 124, $NaHCO_3$ 26, $NaH_2PO_4$ 1.25, KCl 3, D-glucose 10, $MgSO_4$ 1, $CaCl_2$ 2, bubbled with 95%$O_2$ 5% $CO_2$ with a final pH of ~7.4.

**Hypercapnic (55 mmHg $CO_2$) aCSF contained in (mM):** NaCl 100, $NaHCO_3$ 50, $NaH_2PO_4$ 1.25, KCl 3, D-glucose 10, $MgSO_4$ 1, and $CaCl_2$ 2. Solution was saturated with 9% $CO_2$ (with the balance being $O_2$) with pH maintained to match control (35 mm Hg).

**Hypocapnic (20 mm Hg $CO_2$) aCSF contained in (mM):** NaCl 140, $NaHCO_3$ 10, $NaH_2PO_4$ 1.25, KCl 3, D-glucose 10, $MgSO_4$ 1 and $CaCl_2$ 2. Solution was saturated with 2% $CO_2$ (with the balance being O2), with pH maintained to match control (35 mm Hg).

**Stimulation Protocols**

**Standard IV protocol**

A standard current-voltage relationship was constructed by injecting step currents (3 s duration, every 5 s) starting at -200 pA and then incrementing by either 50 or 100 pA until a regular firing pattern was induced. A plot of step current against voltage response around the resting potential was used to measure the input resistance (gradient of the fitted line).

**Naturalistic current injection**

The naturalistic current was generated using the summed numerical output of two Ornstein–Uhlenbeck processes (Uhlenbeck & Ornstein, 1930) with time constants $\tau$fast = 3 ms and $\tau$slow = 10 ms. This naturalistic current waveform (as in Badel et al, 2008), which mimics the stochastic actions of AMPA and GABA-receptor channel activation, was injected into cells (40 s duration) and the resulting voltage recorded (as a fluctuating noisy trace). This voltage trace was then used to evaluate the frequency of action potential firing.

**Current Injection to assess conductance changes**

A hyperpolarising step of 50 pA (100 ms) was injected at a frequency of 1 Hz. This allowed the time course of changes in input resistance/conductance to be assessed. For analysis, averages were constructed for 10-minute periods in 35 mm Hg and 55 mmHg $CO_2$ (when the effects of $CO_2$ had reached steady state).

**For each recording, once whole cell breakthrough had occurred cells were allowed to equilibrate for a few minutes. Following this a standard IV curve was constructed and naturalistic current traces were injected to enable the measurement of firing rate. After these measurements had been recorded (5-10 mins post- whole cell breakthrough), the hyperpolarising step current was initiated to look for voltage changes in response to altered levels of carbon dioxide (from 35 mm Hg to 55 mm Hg, isohydric).**

**Immunohistochemistry**

Mice (P7-10 and P17-20) were cardiac perfused with 4% PFA and then post-fixed overnight at 4ºC. The tissue was washed with PBS and then sliced coronally (350 μm). The slices were left to recover for 1 hour and then were blocked for an hour (1% BSA, 0.4% Triton 100X in PBS, 400 μl per slice) then washed 3 times for 5 minutes with PBS. The primary antibodies against tyrosine hydroxylase, (1:1000, Sheep), GFAP (1:1000, Chicken) or GAD65/67 (1:1000, Rabbit) and the primary antibody against connexin 26 (1:200, Mouse) were added to the slices (400 μl per slice) for an hour at room temperature and then kept at 4-8ºC overnight. Slices were washed 5 times for 5 minutes with PBS and the corresponding secondary antibody (anti-sheep 488, 1:500, anti-mouse 594, anti-sheep 594, anti-chicken 488 or anti-rabbit 488, 1:500, 400 μl per slice) added for 4 hours at room temperature. The slices were then washed 5 times for 5 minutes with PBS, and then mounted on glass slides with Vectashield (Vector laboratories, Peterborough UK). All imaging was carried with confocal microscopy (Leica 710 and Zen Black for image acquisition and processing). Controls were carried out without the primary antibodies and showed no fluorescence.

**Dye loading**

The dye loading method is based on that described in Huckstepp et al (2010). Briefly, a slice was transferred to the recording chamber, submerged and perfused (2-3 ml/min$^{-1}$) with control aCSF (35 mmHg $CO_2$) at 30 °C. Slices were visualized using IR-DIC optics with an Olympus BX151W microscope (Scientifica, Bedford UK) and a CCD camera (Hitachi). To confirm the correct location for imaging, whole cell patch clamp recordings were used to identity DNs and GABAergic neurons in the SN and VTA (Fig. 1 and 4). Slices were then allowed to equilibrate for 20 minutes. The control aCSF was then exchanged for 55 mmHg $CO_2$ aCSF (hypercapnic) containing 5(6)-carboxy-fluorescein (CBF, 100 μM) for 20 mins to allow the $CO_2$ sensitive-hemichannels to open. The solution was then exchanged for 35 mmHg $CO_2$ aCSF containing CBF (100 μM) for 5 minutes to allow the hemichannels to close. Finally, the slice was washed with 35 mmHg $CO_2$ aCSF for 3 hours to reduce the background staining before imaging. Images were taken using the CCD camera (Hitachi) with 488 nm fluorescence (CoolLED). As CBF rapidly bleaches, images were quickly acquired from regions of interest. CBF cannot be fixed using PFA (as it lacks the required groups for cross-linking).

**Statistics**

Data is represented as mean and standard error of the mean with individual experiments represented by single data points. Appropriate statistical tests were chosen based on sample size, whether there were repeated measures and whether the populations were paired or unpaired (Wilcoxon rank sum/ paired t-tests and Mann Whitney tests respectively). For tests of more than two variables, Kruskal-Wallis ANOVAs were run with Dunn's post hoc multiple comparisons. All tests were run to find significance at the level $p < 0.05$ and were performed on raw (non-normalised) data, available in supplementary data (figures 5-8).